Experimental Cell Research 340 (2016) 71–80

Contents lists available at ScienceDirect

Experimental Cell Research

journal homepage: www.elsevier.com/locate/yexcr

Research article

FTIR microspectroscopy defines early drug resistant human hepatocellular carcinoma (HepG2) cells

Cholpajsorn Junhom [a], Natthida Weerapreeyakul [b,*], Waraporn Tanthanuch [c], Kanjana Thumanu [c]

[a] Biomedical Sciences Program, Graduate School, Khon Kaen University, Khon Kaen 40002, Thailand
[b] Faculty of Pharmaceutical Sciences, Khon Kaen University, Khon Kaen 40002, Thailand
[c] Synchrotron Light Research Institute (Public Organization), Nakhon Ratchasima 30000, Thailand

ARTICLE INFO

Article history:
Received 10 July 2015
Received in revised form
1 December 2015
Accepted 15 December 2015
Available online 18 December 2015

Keywords:
FTIR microspectroscopy
Resistance cancer cells
Hepatocellular carcinoma
Efflux proteins
Biochemical change

ABSTRACT

Characterization and identification of cancer cell, chemotherapy, resistance is important for both routine cancer therapy and trouble-shooting the medication treatment regimen. Present techniques for characterizing cancer cell resistance require multiple methods and steps, which are time-consuming and expensive. We present a protocol for simple sample handling, rapid detection, and spectral characterization of early resistant hepatocellular carcinoma (HepG2) cells, using Fourier transform infrared microspectroscopy (FTIR). Studies on alteration of the biochemical properties in a resistant HepG2 cell were evaluated—viz., increase efflux proteins (MRP-1 and P-gp) activity, total GSH content, anti-apoptotic (Bcl2) expression, and reduction of pro-apoptotic (Bax) proteins. Principle component analysis (PCA) was used to discriminate resistant HepG2 cells from parental HepG2 cells. Three important FTIR spectral regions were evaluated for reproducibility and discrimination ability—viz., lipid (3000–2800 cm^{-1}), protein (1700–1500 cm^{-1}) and carbohydrate and nucleic acid (1300–900 cm^{-1}). These 3 spectral regions can be used as spectroscopic biomarkers for differentiation of early or low resistance. This work presents a novel concept for high-throughput, FTIR spectroscopic discrimination of early resistance; thus enabling identification and characterization of cancer cell resistance.

1. Introduction

Hepatocellular carcinoma (HCC) is a major liver cancer, accounting for one-third of cancer mortality worldwide [1,2]. The underlying causes of HCC are chronic infections with Hepatitis B and C viruses, mycotoxin-contaminated food (aflatoxins), alcoholic liver disease and non-alcoholic fatty liver disease [3]. The treatment for HCC depends on the stage of cancer and includes resection, transplantation, trans-arterial chemoembolization, percutaneous ethanol injection therapy, radiofrequency ablation, chemotherapy, and molecular targeted therapy [3]. The continuous rise in the prevalence of HCC and its high mortality—with an average survival of < 12 months with advanced HCC—indicates the insufficiency of early detection and the lack of any cure [4]. Despite the combinations of chemotherapeutic drugs recommended, the problem of severe toxicity of the drugs [5] and cancer resistance [6] limit the efficacy of treatment protocols.

Multidrug resistance (MDR) is also a significant problem for cancer therapy, leading to low efficacy of chemotherapeutic drugs. The commonly reported resistance mechanisms include (a) overexpression of efflux pump (i.e., P-glycoprotein and MRP family), leading to less drug accumulation inside cancer cells [5]; (b) overexpression of enzymes (i.e., the glutathione detoxification system) leading to higher drug metabolism [7]; and, (c) imbalanced protein expression/function between anti- and pro-apoptotic proteins [8]. The diversity of genetic and molecular changes alter the response to cellular drug targets, lessening the concentration reaching the target or undermining successful chemotherapeutic treatment [9]. Despite advances in technology and cancer research, conventional chemotherapy and other systemic treatments have been largely ineffective.

Early detection of the cancer stage is critical to patient survival and effective treatment. In the early stages of cancer, the cancer cells can respond to chemotherapeutic drugs; however, the cells cannot be completely removed from the body after metastasis and the sensitive cancer cells (now immortalized) become resistant to treatment. Most current anticancer therapies—including chemotherapy, radiotherapy, and immunotherapy—primarily work by

* Correspondence to: Faculty of Pharmaceutical Sciences, 123 Mittrapap Road, Amphoe Muang, Khon Kaen University, Khon Kaen, 40002, Thailand.
E-mail addresses: cholpajsorn_j@hotmail.com (C. Junhom), natthida@kku.ac.th (N. Weerapreeyakul), waraporn@slri.or.th (W. Tanthanuch), kanjanat@slri.or.th (K. Thumanu).

http://dx.doi.org/10.1016/j.yexcr.2015.12.007
0014-4827/

activating cell death pathways, including apoptosis in cancer cells. Human cancers can, however, develop intrinsic or acquired resistance to apoptosis. One widely used diagnostic method—for the clinical assessment of cancers—is microscopic evaluation of a stained biopsy from specific tissues, but this can be inaccurate and/or costly [10]. Various efforts have, therefore, been made to improve early detection of resistant cancer cells.

Fourier transform infrared (FTIR) microspectroscopy is an absorption spectroscopy technique for demonstrating the cellular biochemical composition or tissue components [11]. Notable benefits of FTIR include that it is: (a) non-destructive without labeling; (b) highly sensitive; (c) a specific and powerful analytical technique [12]; (d) fast; (e) inexpensive; and, (f) that it has a acquisition time. The FTIR is thus useful for determination of several cell states with the advantages of a rapid measuring process and high spatial resolution [13–17]. This technique enables the study of the state of chemical bonds and the relative concentrations of cellular biochemical components. The obtained FTIR spectra define characteristic of lipid, protein, carbohydrate, and nucleic acid regions. Based on this principle, several applications of FTIR have been reported for cancer diagnosis [18] and distinguishing cancer cells from normal cells (e.g., malignant colon cancer [18], lung cancer [10], ovarian tumor [19], breast cancer [20], esophageal cancer [21], malignant human hepatocytes [22]. FTIR microspectroscopy has, moreover, been used to discriminate between resistant and parental cancer cells, such as in ovarian tumor [19], human melanoma cell lines [23], human leukemic (K562) cell lines [24], uterine sarcoma cell lines [25], and ovarian cell lines [26]. To date, however, no application of the FTIR microspectroscopy for detection of resistant HCC is available. A simple, cost-effective and less time-consuming method of FTIR microspectroscopy is, therefore, of considerable interest.

This is the first report of an application of FTIR microspectroscopy on detection of biochemical changes in the resistance HepG2 cells vs. parental HepG2 cells. We provide the evidence of its benefit to cancer treatment against conventional methods, which require many diagnostic steps. The critical outcome of our study was finding that FTIR microspectroscopy is a highly sensitive technique for rapidly detecting the initial stages of resistant cancer cells.

2. Materials and methods

2.1. Chemicals

Human hepatocellular carcinoma (HepG2) cells (ATCC#8065) were prepared with Dulbecco's Modified Eagle Medium (DMEM). The reagents used in the cell culture techniques were biological grade and were bought from GIBCO, Invitrogen Corporation (Grand Island, NY, USA). Neutral red was purchased from Sigma Aldrich Co. (St. Louis, MO, USA). Cisplatin was purchased from Boryung pharmaceutical Co., Ltd. (Kyungki-do, Korea). R(+)-verapamil monohydrochloride hydrate, rhodamine 123, 5(6)-carboxyfluorescein diacetate, and probenecid were purchased from Sigma Aldrich Co. (St. Louis, MO, USA). The glutathione assay kit was purchased from Abnova (Redfern NSW, Australia). The primary antibodies—Bax, Bcl-2 and β-actin—were purchased from Santa Cruz Biotechnology (Dallas, Texas, USA). The goat anti-mouse IgG1 heavy chain (horse radish peroxidase) was performed with Abcam (Cambridge, UK). Enhanced chemiluminescence (ECL) reagent was bought from GE Healthcare UK Limited (Buckinghamshire, UK).

2.2. Cell culture

Adherent HepG2 (human hepatocellular carcinoma cells) were grown in Dulbecco's Modified Eagle Medium (DMEM) supplemented with 10% fetal bovine serum (FBS) and 1% penicillin-streptomycin. The cells were maintained in 5% CO_2 incubator at 37 °C.

2.3. Development of cisplatin resistant HepG2 cells

The induction of drug resistance in cancer cells was repeated by a stepwise increase of cisplatin concentration exposure to the parental HepG2 cells [27]. Briefly, HepG2 cells were exposed to cisplatin at a starting dose of 1.0 μg/ml for 24 h. After induction, the drug in the medium was removed. The HepG2 cells were washed by (1x) PBS and cultured in the complete medium. Cells were grown in the media until 80% confluency. The HepG2 resistance to cisplatin was developed by increasing the dose from 1.0 μg/ml to 1.6 μg/ml to 2.1 μg/ml to 2.4 μg/ml. This process was repeated until resistance was achieved. The IC_{50} was determined as the drug concentration having 50% cell growth inhibition in comparison to the untreated cells or control group. The resistance index (RI) was calculated from the ratio of the IC_{50} of cisplatin in the resistant HepG2 cells divided by the IC_{50} of cisplatin in the parental HepG2 cells. Before all experiments, the cultures were restarted from frozen stocks (−80 °C) and cultured to 80% cell confluence.

2.4. Cisplatin sensitivity study

The drug sensitivity of the parental and resistant HepG2 cells to cisplatin drug was performed based on neutral red (NR) assay [28], which approximates cell viability. NR is a cationic dye that can penetrate into viable cells, incorporate and bind with lysosomes of the viable cells. The viable cells can, therefore, be measured by spectrophotometer. Briefly, the cells were cultured in T25 flasks in a 5% CO_2 incubator. After cells reached about 70–80% confluence, cells were seeded at a density 4×10^4 cells/ml in a 96-well plate in the complete medium, and were incubated for 24 h. Then, the fresh media containing various concentrations of cisplatin solution were added and incubated for another 24 h. The control experiment was the untreated cells, which only contained the complete medium and cells. NR solution in media was added to each well to give a final concentration of 50 μg/ml and incubated for 2 h at 37 °C in a 5% CO_2 incubator. Cells were then washed with 1x PBS and were solubilized with 0.33%v/v HCl in isopropanol. The viable cells with NR were measured using a microplate reader (Tecan's Sunrise™ absorbance reader, Austria) for absorbance at dual wavelengths (viz., 537 nm and 650 nm). The % cell viability was calculated as $[A_{test}/A_{control}] \times 100$; when $A_{control}$ = Absorbance of control (untreated cells) and A_{test} = Absorbance of test (treated cells).

2.5. Functional assay of P-gp activity

The presence of the efflux proteins in resistant HepG2 cells was determined from the P-gp activity following the method by Okura [29] with minor modifications. Briefly, after reaching 80% cell confluence, cells were seeded into sterile a 24-well plate at 1×10^6 cells/ml and cultured for 24 h at 37 °C in 5% CO_2 incubator. Cells were pre-incubated with fresh media in the absence or presence of 30 μM verapamil (an inhibitor of P-gp) for 30 min. After the pre-incubation, 10 μM rhodamine 123 (a fluorescent P-gp substrate) was added to each well. Then, cells were incubated for 60 min at 37 °C in a 5% CO_2 incubator. After this final incubation, the cells were washed twice with an ice-cold phosphate-buffered saline (1 × PBS), pH 7.4. Cells were re-suspended with 1x PBS. The accumulation fluorescence of rhodamine 123 was detected by using flow cytometry (BD FACSCanto II, Franklin Lakes, NJ, USA) at wavelengths of 488 and 530 nm, respectively.

2.6. Functional assay of MRP-1 activity

The activity of the MRP-1 efflux protein was determined following the method of [30] with slight modifications. In this study, carboxyfluorescein diacetate (5(6)-CFDA) acted as a specific substrate for MRP-1 and probenecid acted as a MRP-1 inhibitor. Briefly, cells were seeded into a sterile 24-well plate at 1×10^6 cells/ml and cultured for 24 h at 37 °C in a 5% CO_2 incubator. Cells were pre-incubated with fresh media in an absence or presence of 1 mM probenecid for 30 min. After the pre-incubation, 5 μM of CFDA was added into each well. Then, cells were incubated for 60 min at 37 °C in a 5% CO_2 incubator. The cells were washed twice with an ice-cold phosphate-buffered saline (1 × PBS), pH 7.4. Cells were re-suspended with 1 × PBS. The accumulation fluorescence of CFDA was detected by using flow cytometry (BD FACSCanto II, Franklin Lakes, NJ, USA) at wavelengths of 488 and 530 nm, respectively.

2.7. GSH detoxification

The total Glutathione (GSH) was analyzed using a glutathione assay kit (colorimetry). Cells were lysed with ice-cold Glutathione buffer and incubated on ice for 10 min. The cells were centrifuged at 8000*g* for 10 min and the supernatant was collected. The glutathione assay was performed on the supernatant. NADPH generating mix, glutathione reductase, and glutathione reaction buffer were prepared for the reaction mixture and added to the well and incubated at room temperature to generate NADPH. Sample or standard were added to the reaction mix. Finally, the substrate was added and the total amount of glutathione was measured by the absorbance at 405 or 415 nm using a microplate reader.

2.8. Apoptosis induction by using flow cytometry

After being treated with 5 μg/ml cisplatin, apoptotic death mode was determined in the resistant HepG2 cells and the parental HepG2 cells at 12 and 24 h. The mode of cell death was determined using double staining annexin V and propidium iodide binding, following the manufacturer's instructions (Biolegend Inc., San Diego, CA, USA) with slight modifications. Annexin V can bind to the surface of early membrane-intact apoptotic cells, while propidium iodide stains the disrupted internal and external membranes of necrotic cells. Parental and resistant HepG2 cells were cultured in 24-well plates. The cells in each well were treated with 5 μg/ml of cisplatin for 12 and 24 h. After incubation, cells were trypsinized, washed, and suspended cells with cold staining buffer. The suspension cells were centrifuged and the supernatant discarded. Then cells were re-suspended in binding buffer. The 5 μl of Annexin V was added to cells followed by 10 μl of propidium iodide. Cells were then gently vortexed and incubated for 15 min at room temperature (in the dark). After incubation, cells were analyzed within 2 h after staining using flow cytometry (BD FACSCanto II, BD Biosciences, San Jose, CA, USA).

2.9. Protein expression

Cells were lysed in a NP-40 buffer [150 mM NaCl, 1% Triton X, 50 mM Tris (pH 8), 5 mM EDTA] and incubated for 1 h at −20 °C. The lysate was centrifuged at 32,869 *g* for 15 min, 4 °C and the supernatant stored at −20 °C. Protein concentrations were determined using a BCA assay kit. Forty micrograms of proteins plus 5x sample buffer [1 M Tris (pH 6.8), sodium dodecyl sulfate, bromophenol blue, dithiothreitol) were boiled at 100 °C for 5 min. The samples were loaded and separated by electrophoresis in 12.5% polyacrylamide gel (SDS-PAGE). Western blotting was done on the separate proteins, which were transferred to polyvinylidene difluoride (PVDF), and blocked with 5% nonfat milk for 2 h. The membrane was then incubated with the primary antibodies overnight at 4 °C [diluted: Bax (1:200), Bcl-2 (1:500)] and β-actin (1:1000) used for normalization. This membrane was washed with TBS-tween buffer every 10 min thrice then incubated in goat anti-mouse IgG1 heavy chain (horse radish peroxidase) for 2 h. The membranes were washed with TBS-Tween buffer every 10 min thrice. Finally, the band was observed using chemiluminescence in conjunction with enhanced chemiluminescence (ECL) reagent [31].

2.10. Sample preparation for FTIR analysis

The parental and resistant HepG2 cells were trypsinized and centrifuged at 540 g for 5 min. These cells were washed using 0.9% of NaCl (w/v) twice and re-suspended in 50 μL of 0.9% of NaCl (w/v). This step was gently performed and the abrupt change between the osmolarity of the culture media and the physiological saline solution did not occur. The re-suspended cells were transferred onto Low-e Microscope Slides (MirrIR, Kevley Technologies, Chesterland, OH, USA) and vacuum-dried for 30 min in a desiccator [13,14]. The cells on the slide were rinsed with distilled water then vacuum-dried. This step was repeated to completely remove the salt. The washed and dried cell monolayer was stored in a desiccator until used.

2.11. FTIR microspectroscopy and unsupervised explorative multivariate data analysis

FTIR experiments were conducted at the IR end station of Synchrotron Light Research Institute (Public Organization), Thailand. Samples were analyzed in transflection mode, using the conventional internal IR source of a Bruker Vertex 70 spectrometer connected to the Bruker Hyperion 2000 microscope (Bruker Optics Inc., Ettlingen, Germany). The microscope—with a 36 × objective/condenser—was equipped with a nitrogen-cooled MCT (HgCdTe) detector (area 250 × 250 μm^2). IR signals were acquired from 60 to 70 cells comprised within 68 × 68 μm^2 spot areas, mapped within most homogeneous zones. Sixty-four scans (20 kHz velocity and 4 cm^{-1} spectral resolution) were performed within the 4000–600 cm^{-1} spectral interval in order to obtain the average spectra with an appropriate signal-to-noise ratio. OPUS 6.5 software (Bruker) enabled the instrumental control, sample stage movements, spectral acquisition, and the post-acquisition processing of raw spectra from which CO_2 and water vapor were subtracted before calculating the mean integral values of the selected peak area (the area above a straight line drawn between the two frequency limits defining the peak). Integration was applied to the following intervals. The anti symmetric and symmetric CH stretching from membrane lipids (3000–2800 cm^{-1}) (Supplement Table 1). The absorbance of protein amide I and amide II vibrational modes (1700–1500 cm^{-1}). The absorbance of functional groups (1300–900 cm^{-1}) in nucleic acids DNA and RNA, carbohydrates, phospholipids, proteins and phosphorylated proteins, which cannot be unequivocally assigned because of their partial overlapping.

Unsupervised explorative multivariate data analysis by Principal Component Analysis (PCA) was conducted using variables within the 3000–2800 cm^{-1} and 1800–900 cm^{-1} intervals. Variability related to variable baseline, different sample thickness, and scattering artifacts were minimized by normalization with extended multiplicative signal correction (EMSC) and the calculation of second derivative spectra with the Savitzky-Golay algorithm using 9 points of smoothing (Unscrambler 9.7 software, CAMO, Oslo, Norway). Six PCs were considered for classification analysis using a Non-linear Iterative Partial Least Squares (NIPALS) algorithm with leverage correction to estimate model stability and

predict full cross-validation. The constant value of the weighting for all variables was set to 1.

2.12. Statistical analysis

The results were expressed as mean ± SD and the statistical differences between treatments were tested using the *t*-test. Differences in p values < 0.05 were considered statistically significant.

3. Results and discussion

3.1. Cell morphology and cisplatin sensitivity in parental and resistant HepG2 cells

The development of multidrug resistance (MDR) is a common problem in patients treated with intermittent chemotherapy. The availability of ex vivo MDR cell line models is thus key to studying the characteristics and mechanisms of drug resistance [32]. Drug resistance induced by intermittent exposure of cells to anticancer agents has been reported to have more clinical relevance than that obtained by continuous exposure [32]. Cisplatin has been used widely as a chemotherapeutic drug for a variety of malignancies including HCC [33]. Here we used the intermittent method to generate cisplatin-resistant HepG2 cell sub-clone from cells initially sensitive to this anticancer agent. Initially, HepG2 cells with cisplatin induced-resistance reached 80% cell confluence within 10 days while parental HepG2 cells took only 3 days. As the MDR population of HepG2 cells was increasing, the proliferation rate approached that of cisplatin-sensitive control HepG2 cells while the percentages of viable cells detected in samples exposed to increasing concentration of cisplatin was significantly higher in the drug resistant than the drug sensitive HepG2 sub-clones (Fig. 1C).

Structural and functional changes paralleling the acquisition of chemo-resistance have been described—in particular cell shape and cytoskeleton reorganization, the fluidity of plasma membrane influencing surface tension and cell stiffness, and enabling cancer cell with an invasive pattern to spread into other tissues [34]. Fig. 1A and B shows parental and resistant HepG2 cells in culture medium as observed under the bright field inverted microscope (10 ×). No significant change of cellular morphology can be observed between the two cell populations and both cell lines appear to have very similar epithelial-like morphology with close cells. In the early stages of resistance, cell morphology cannot distinguish cisplatin sensitive from cisplatin resistant HepG2 cells with significantly higher IC_{50} values (IC_{50}: 4.7 ± 0.2 μg/mL vs. 8.7 ± 0.3 μg/ml, $P < 0.05$) and with a mean resistance index (RI) value of 1.8 (Fig. 1C). Similar levels of resistance were moreover measured in the sub-clone of cisplatin-resistant HepG2 cells cultured in a drug-free medium for 1 month (data not shown). Although morphology did not distinguish sensitive and resistant cells, some molecular biochemical change within the cells might have existed leading to the failure of the chemotherapy were investigated at the molecular level. On the contrary, different FTIR patterns reflected subtle biochemical, structural and metabolic differences between sensitive and resistant HepG2 cells, allowing their correct classification by unsupervised multivariate principal component analysis (PCA). The results of complementary investigations conducted using independent methods cross-validated interpretation of the PCA results.

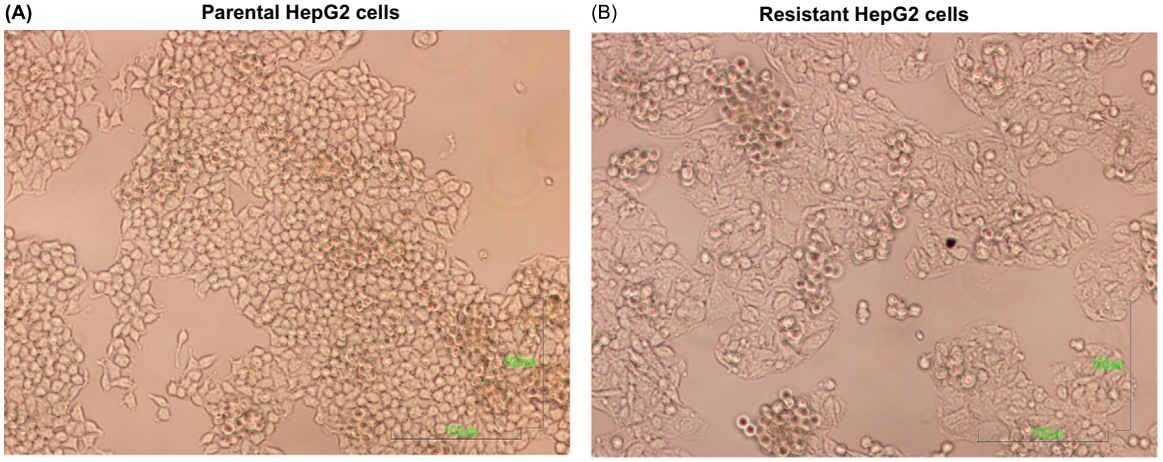

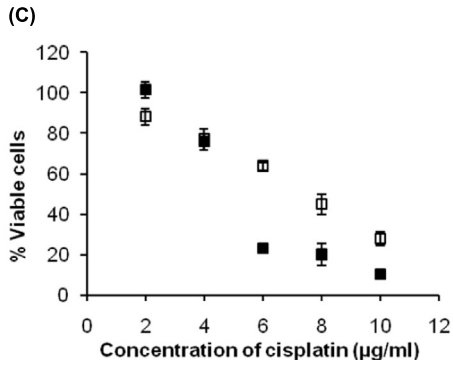

IC_{50} (μg/ml)		RI
Parental HepG2 cells	Resistant HepG2 cells	
4.7±0.2	8.7±0.3	1.8

Fig. 1. Morphology of (A) parental HepG2 cells compared to (B) resistant HepG2 cell subline under bright field inverted microscope (10 ×). (C) Cell proliferation profile of parental HepG2 cell line (■) and resistant HepG2 subline (□) treated with various concentrations of cisplatin for 24 h. Inset represents concentration of cisplatin that exerted 50% anti-proliferation (IC_{50}) in each cell line. Resistance index (RI) indicates IC_{50} value of cisplatin resistance vs. parental HepG2 cells.

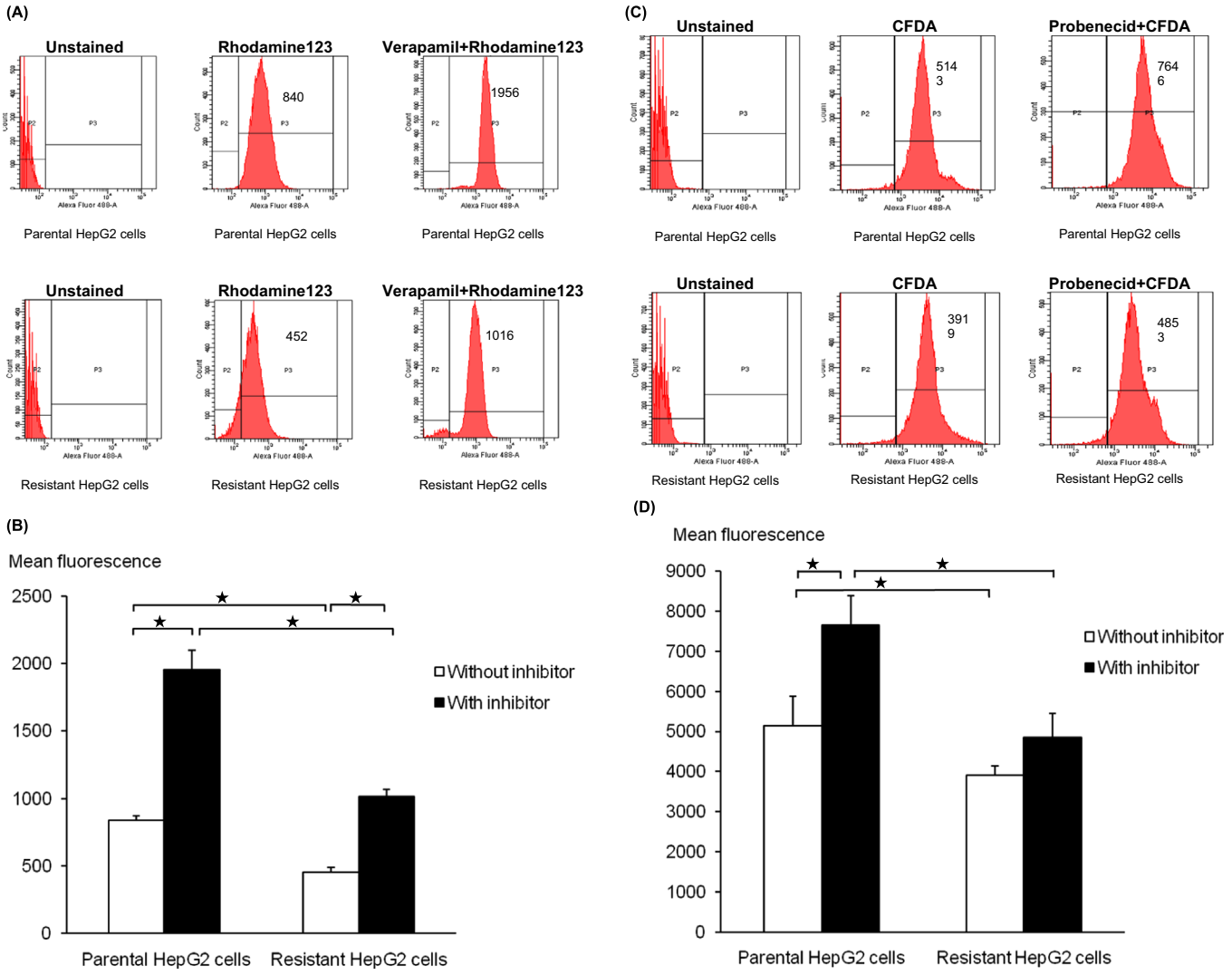

Fig. 2. (A) Flow cytogram represents effect of verapamil (a P-gp inhibitor) on accumulation of rhodamine 123 in parental HepG2 cells and resistant HepG2 cells. (B) Mean fluorescence of rhodamine 123 uptake into parental and resistant HepG2 cells after pre-incubating in presence (■) or absence (□) of verapamil. Each value represents mean ± SD ($n=3$). ★$p<0.05$ (paired t-test) indicates significant difference. (C) Flow cytogram represents effect of probenecid (a MRP1 inhibitor) on accumulation of CFDA in parental HepG2 cancer cells and resistant HepG2 cells. (D) Mean fluorescence of CFDA in individual parental and resistant HepG2 cells after pre-incubating with (■) or without (□) probenecid. Each value represents mean ± SD ($n=3$). ⋆$p<0.05$ (t-test) indicates significant difference.

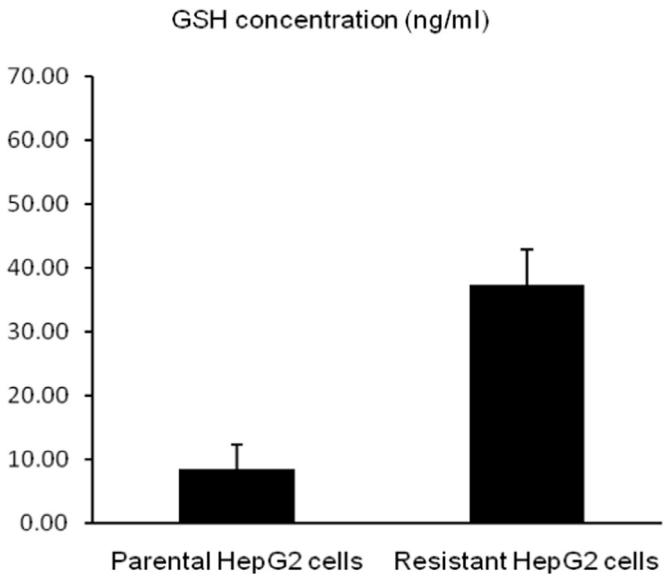

Fig. 3. Total of glutathione (GSH) in parental and resistant HepG2 cells.

3.2. Efflux protein activity

The imbalance of efflux proteins could be responsible for the accumulation of cisplatin inside cancer cells. Both the ATP binding cassette (ABC) family of ATPase (i.e., the P-glycloprotein, P-gp) and the ABC ATPase (i.e., multidrug resistance protein, MRP-1) can increase cisplatin export [35]. P-gp and MRP-1 are two efflux proteins over-expressed in resistant hepatocellular carcinoma cells [36]. Rhodamine 123 and carboxyfluorescein diacetate (5(6)-CFDA) are two fluorescent substrates used to measure the activity of P-gp and MRP-1 efflux proteins in cells, respectively [37]. P-gp activity was evaluated in both resistant and parental HepG2 cells pre-incubated or not with the P-gp inhibitor verapamil. The mean rhodamine 123 fluorescence always resulted ~2-fold higher in parental than in cisplatin-resistant HepG2 cells, independent of inhibition of P-gp activity with verapamil (Fig. 2A and B), providing evidence that P-gp efflux proteins were more expressed and/or their functioning was higher in resistant than in parental HepG2 cells sub-clones.

The fluorescent CFDA dye extrusion indicates MRP-1 efflux activity can be inhibited in cells exposed to the MRP-1 inhibitor probenecid. The results of Fig. 2C and D show that higher CFDA-

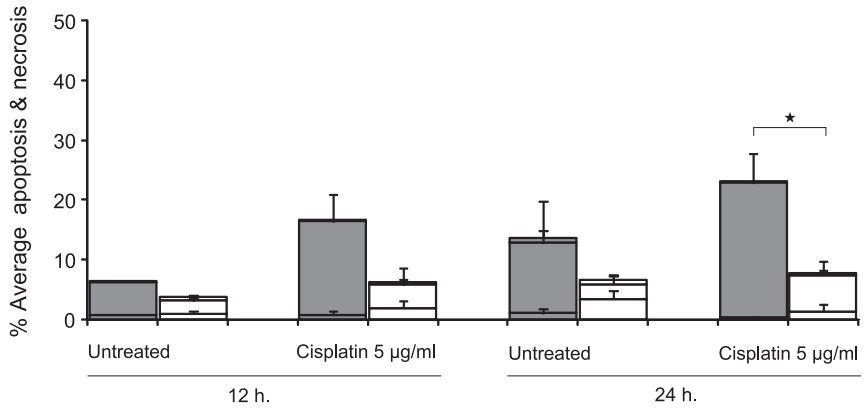

Fig. 4. Respective percentage of apoptotic cells in necrosis (lower bar), early (middle bar) and late stage apoptosis (upper bar) compared to total cell population. Both parental (■) and resistant HepG2 cells (□) treated with 5 μg/ml cisplatin for 12 and 24 h. *Statistically significant difference compared to control ($p < 0.05$).

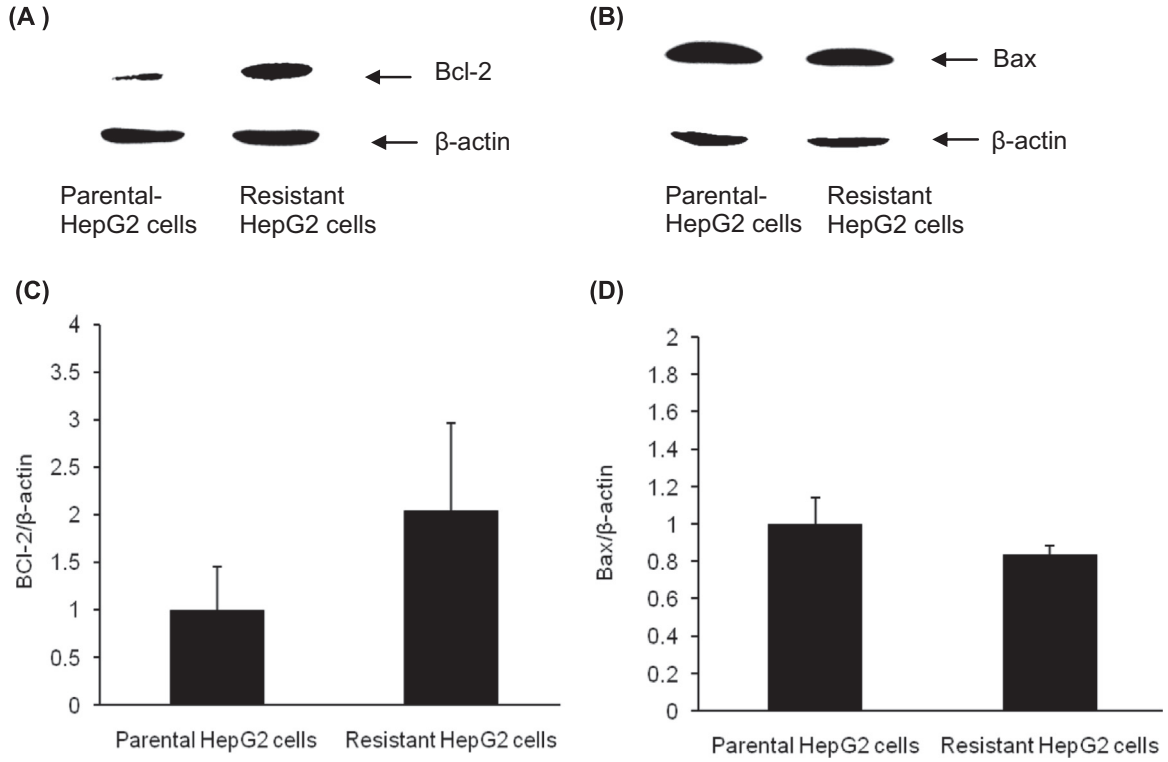

Fig. 5. Western blotting for expression of (A) Bcl-2 and (B) Bax in parental HepG2 cells and resistant HepG2 cells. Sequential incubation of blots with β-actin antibody confirmed equal protein loading. Data represents 3–5 different experiments. (C) Bcl-2/β-actin ratio and (D) Bax/β-actin ratio obtained from corresponding western-blots.

related fluorescence is retained in parental than in resistant HepG2 cells and this significant difference can be still observed in cells pre-incubated with probenecid thus suggesting that also MRP-1 over-expression—and its related extrusion activity—was higher in cisplatin-resistant than in parental HepG2 cells. The concentrations of verapamil and probenecid did not affect cell viability in samples (data not shown). Cytotoxicity, impaired DNA repair and decreased levels of cisplatin-inactivating factors (e.g., glutathione and metallothioneins) might explain the anticancer activity associated with intracellular accumulation of cisplatin in cancer cells [38]. Decreased cisplatin accumulation—resulting from increased efflux and/or decreased retention or both, as our results suggest—can contribute to cisplatin-resistance in HepG2 cells. It should be noted that both P-gp [35,36,38] and MRP-1 [37] protein structure have relatively high percentages of α-helical structures that can be studied by FTIR spectroscopy in pure protein samples [39].

3.3. GSH detoxification

Compared to parental control HepG2, higher levels of GSH were measured in cisplatin-resistant HepG2 cells (Fig. 3). The nucleophilic molecule of GSH reacting with the electrophilic molecule of cisplatin can inactivate the effects of this anticancer drug, which can be better extruded from cells through the MRP-1 efflux protein pathway. The high GSH might also be implicated in the mechanisms of cisplatin resistance in cancer cells.

3.4. Apoptotic cell death

The percentage of apoptotic cells (early and late) detected by flow cytometry (Fig. 4) increased in a time-dependent manner and resulted in significantly lower resistant HepG2 than parental HepG2 cells after exposure to 5.0 μg cisplatin/ml for 24 h (Fig. 4, *t*-test, $p < 0.05$).

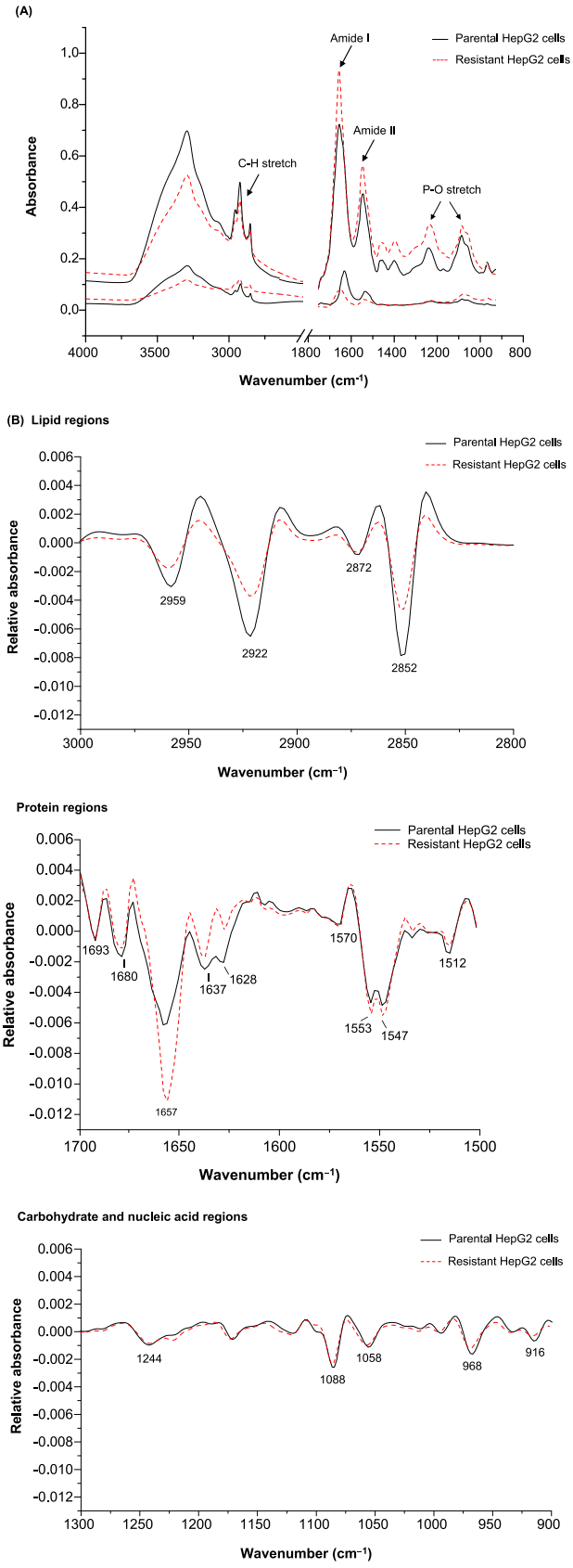

Fig. 6. (A) Average absorbance spectra with their standard deviation and (B) second derivative FTIR spectra of 2 cell samples: solid black line (–) represents parental HepG2 cells and dashed red line (—) resistant HepG2 cells. (A) 78 spectra of parental HepG2 cells and 117 spectra of resistant HepG2 cells accounting for differences in sample thickness normalized with extended multiplicative signal correction (EMSC). Assigned band in FTIR spectra represent lipid region (3000–2800 cm^{-1}), protein region (1700–1500 cm^{-1}) and carbohydrate and nucleic acids (1300–900 cm^{-1}). (B) Second derivative FTIR spectra shown in 3 different regions; lipid, protein, and carbohydrate and nucleic acid regions. Second derivative spectra processed by taking Savitzky–Golay algorithm and normalizing with multiplicative signal correction (EMSC) and averaging into one spectrum of each sample.

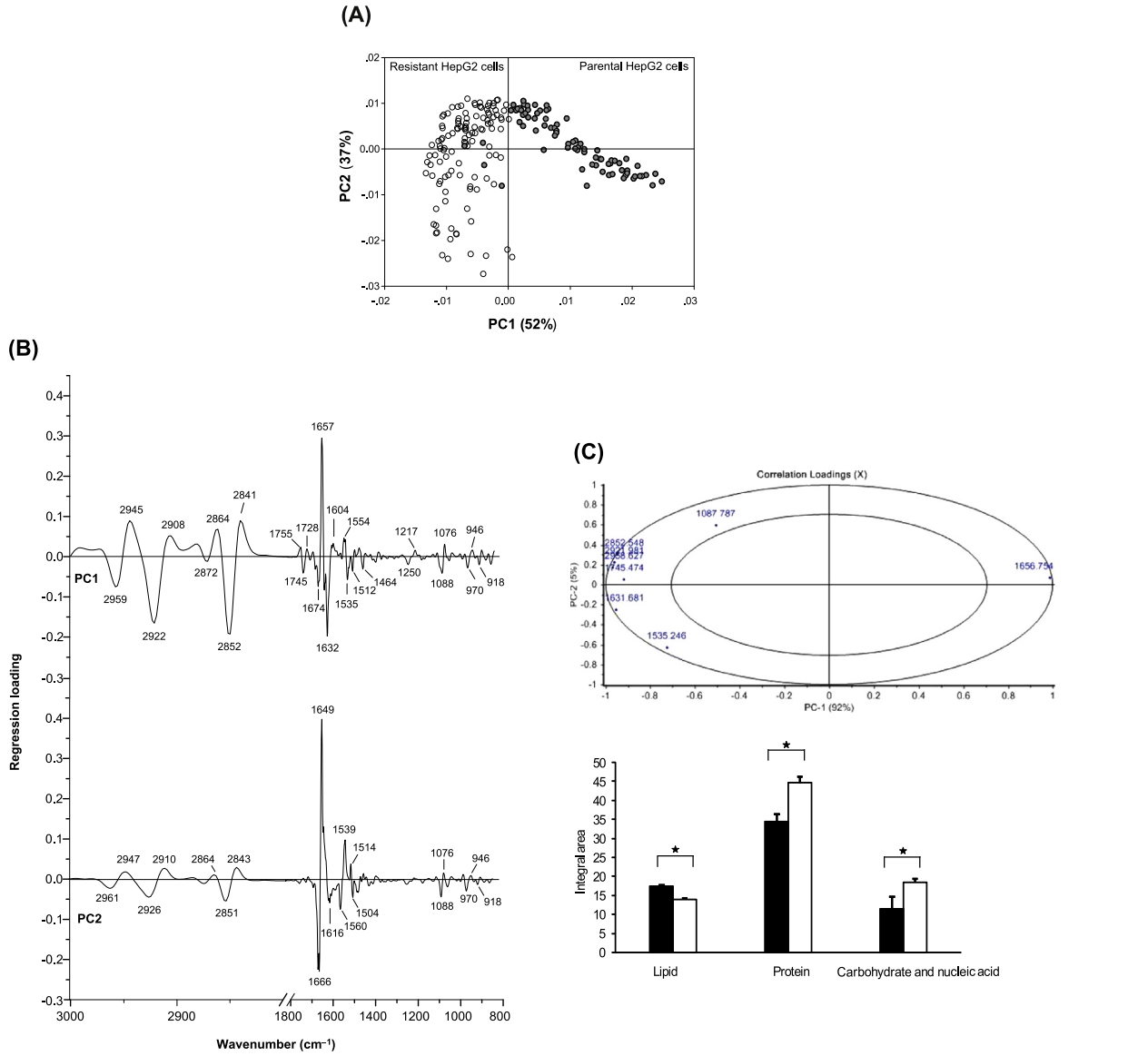

Fig. 7. PCA analysis of FTIR spectral range 3000–2800 and 1800–900 cm^{-1} giving PCA score plots (A) and PCA loading plots (B). PCA score plot of HepG2 cells calculated from second derivative spectra from 117 spectra of resistant HepG2 cells and 78 spectra of parental HepG2 cells, respectively. PCA score plots showed distinct clustering between resistant (○) and parental HepG2 (■) cell lines. PCA loading plots indicate biomarker difference by discriminating wave numbers over spectral range of cell samples. (C) Correlation loading plot corresponding PCA. (D) Histogram represents mean integral areas for lipid (3000–2800 cm^{-1}, protein (1700–1500 cm^{-1}), carbohydrate and nucleic acid (1300–900 cm^{-1}) of parental (■) and resistant (□) HepG2 cells. ★Significant differences between groups ($p < 0.05$, paired *t*-test).

3.5. Protein expression

The over-expression of anti-apoptotic Bcl-2 protein has already been associated with cisplatin resistance in cell lines and the recurrence of cancer [35]. To test whether an imbalance of pro- and anti-apoptotic pathways could enable cancer cells to become resistant to chemotherapy with cisplatin, we determined the expression of both the anti-apoptotic Bcl-2 and pro-apoptotic Bax proteins in sensitive and resistant HepG2 cells. The results presented in Fig. 5 illustrate the increased expression of Bcl-2 and the decreased expression of Bax proteins in cisplatin-resistant HepG2 cells whereas the opposite was observed in cisplatin-sensitive HepG2 cells where Bax was expressed more than Bcl-2.

3.6. Cellular biochemical alteration detected by the FTIR microspectroscopy

Infrared radiation was absorbed by cancer cells; thereby revealing the vibration of covalent bonds of the molecule within the cell sample. The wavelength of absorbed infrared radiation depends upon the nature of the covalent bond and the strength of any intermolecular interactions. As the biochemistry of cells changes during development of resistance, the biochemical fingerprint of resistant cancer cells is unique [18,20]. Using FTIR microspectroscopy [40], the signature of resistant HepG2 cells is detected. Principal component analysis (PCA) was performed to discriminate resistant HepG2 cells from parental HepG2 cells.

The FTIR spectra of the resistant and parental HepG2 cells were acquired between 4000–600 cm^{-1} (Fig. 6A). The respective peak at 2959 cm^{-1}, 1657 cm^{-1}, 1547 cm^{-1}, and 1088 cm^{-1} was assigned to C–H stretch, Amide I, Amide II and P–O stretch. The average FTIR spectra from the two data sets presented a similar pattern comprising (a) a lipid region (3000–2800 cm^{-1}), (b) a protein region (1700–1500 cm^{-1}), and (c) carbohydrate and nucleic acids region (1300–900 cm^{-1}) (Fig. 6A). The average FTIR spectra between the two cell lines were similar in band profile shape but different in total absorbance (Fig. 6A). The mean respective FTIR spectrum was thereafter converted to a second

derivative to eliminate broad baseline slopes in the spectra and overlapping individual bands in the unprocessed spectra. The sharper absorbance and smoother baseline of the second FTIR derivative spectra are presented in Fig. 6B.

3.6.1. Biochemical identification

The average FTIR absorbance spectra of cisplatin-resistant and cisplatin-sensitive HepG2 cells are shown in Fig. 6A (4000–600 cm^{-1}). The 3000–2800 cm^{-1} interval indicates absorbance of specific functional groups characterizing major molecular components such as lipids. The 1700–1500 cm^{-1} interval indicates proteins (amide I and amide II peaks) and phosphate groups in nucleic acids DNA and RNA. To identify the band and sub-band components, the second derivative spectra peaks were analyzed (Fig. 6B). The assignment of vibrations to specific IR frequencies (wave numbers) are summarized in Supplementary Table 1 [11–13,41]. The most obvious quantitative differences were within the 1700–1500 cm^{-1} interval, reflecting vibrations of protein amide I (1700-1600 cm^{-1}) and amide II (1600–1500 cm^{-1}). In particular, the region of amides was utilized to identify and assign vibrations reflecting changes of secondary structures in proteins (e.g., those occurring during the cell cycle and/or cell apoptosis) [12]. It is worth noting the higher absorbance at 1657 cm^{-1} assigned to α-helix in proteins, characterizing the spectrum of cisplatin-resistant HepG2 cells. Other differences were observed within the lipid region and the 1300–900 cm^{-1} interval where the absorbance of functional groups—characterizing carbohydrate, lipids and phospholipids, nucleic acids, cyclic nucleotides and phosphorylated proteins—cannot be unequivocally assigned to specific frequencies.

3.6.2. Discrimination of resistant HepG2 cells from the parental HepG2 cells

PCA provides an interpretable overview of the main information contained in a multidimensional data table where rows are spectra of HepG2 cells and columns are variables (wavenumber within selected intervals). When these are projected into a virtual bi-dimensional space, a smaller number of latent variables—called Principal Components (PC)—can summarize most of the relevant information carried by the original variables. The first PC contains the greatest source of information in the data set and each subsequent PC contains, (in order) less information than the previous one. By maximizing the dispersion of data points (each being a spectrum) in a multi-dimension virtual space, the PCA can be applied (a) to perform multivariate explorative analysis allowing identification of the most relevant variables by the unsupervised method and (b) to separate sample groups (the spectra of parental and cisplatin resistant HepG2 cells).

PCA represents a powerful and objective multivariate data analysis technique generally applied to identify: (1) the most important variables (in this case wavenumber), describing differences between samples; (2) variables giving the major contribution to an observed difference; and, (3) variables contributing in the same way. Two types of information could be achieved by PCA: class separation indicated by scores plot (Fig. 7A) and loading plots, which identifies the variables contributing to the class-specific information responsible for clustering (Fig. 7B). Excepted for a few overlapped spectra, PC1 in the 2D scores plot of Fig. 7A was sufficient to group separately cisplatin-resistant cells from cisplatin-sensitive parental HepG2 cells with an accuracy of 96.5% and explained 52% total variance while PC explained the remaining 37% total variance in the model. The PCA profile—also indicated as "factor loading"—can provide vital clues vis-à-vis the biochemical variations among the different cells [42]. PCA loading plots were used to identify the regions of the FTIR spectrum, which contributed highly to the clustering (Fig. 7B). The cause of the variation pattern is explained in the relation to the loading plot (Fig. 7C). The variables in the radius between the ellipses are more discriminating for the cell samples indicating 100% explained variance (Fig. 7C). The amide I region was affected by the highest variance indicating that quantitative and qualitative differences among secondary structures in proteins could differentiate cisplatin resistance from cisplatin sensitive parental HepG2 cells at the molecular level (Fig. 6B). It is not clear if differences in the secondary structure of proteins can be ascribed to the over-expression/activity of efflux proteins P-gp [43–45] and MRP [46] or rather must be associated with the different percentages of apoptotic cells present within probed areas of sensitive and resistant HepG2 cells samples. Other subtle differences involved variables within the 3000–2800 cm^{-1} interval (lipid region) and the phosphate region (1300–900 cm^{-1}).

4. Conclusions

The current study demonstrated that FTIR microspectroscopy and multivariate statistical analysis (i.e., clustering of data with PCA) represent a simple and precise method for discriminating the biochemical pattern of HepG2 cancer cells resistant to cisplatin. Conceivably, the modifications of secondary protein conformation can reflect the increased expression and activity of efflux proteins and of reduced glutathione-associated drug resistance, enabling the prevalence of anti-apoptotic mechanisms in resistant cells.

The application of FTIR microspectroscopy with a conventional IR source in combination with unsupervised multivariate IR analysis by PCA provides an effective method for classifying the early stages of cisplatin-resistant HepG2 cells. This convenient, rapid, reagent-free approach could be extended to study drug-resistance in tissue samples—from fine needle aspirated cytological or biopsied samples from HCC patients—and considered as a complementary technique useful to explore drug-sensitivity and drug-resistance in early stage cancer.

Conflict of interest

The authors declare that they have no conflicts of interest.

Acknowledgments

CJ was awarded a Ph.D. scholarship and Research Grant from the Synchrotron Light Research Institute (Public Organization) (GS-54-D05). The authors thank Dr. Sirinart Srichan for technical assistance pertaining to the FTIR microspectroscopy and Mr. Bryan Roderick Hamman for assistance with the English-language presentation of the manuscript.

Appendix A. Supplementary material

Supplementary data associated with this article can be found in the online version at http://dx.doi.org/10.1016/j.yexcr.2015.12.007.

References

[1] N. Imai, M. Ishigami, Y. Ishizu, T. Kuzuya, T. Honda, K. Hayashi, et al., Transarterial chemoembolization for hepatocellular carcinoma: A review of techniques, World J. Hepatol. 6 (2014) 844–850.
[2] F.A. Eskens, K.J. van Erpecum, K.P. de Jong, O.M. van Delden, H.J. Klumpen, C. Verhoef, et al., Hepatocellular carcinoma: Dutch guideline for surveillance, diagnosis and therapy, Neth. J. Med. 72 (2014) 299–304.
[3] H.B. El-Serag, Hepatocellular carcinoma, N. Engl. J. Med. 365 (2011) 1118–1127.

[4] B.O. Odii, P. Coussons, Pharmacological isolation of experimental models of drug-resistant hepatocellular carcinoma cell line, J. Cancer Ther. 03 (2012) 216–221.
[5] C.H. Sukowati, N. Rosso, L.S. Croce, C. Tiribelli, Hepatic cancer stem cells and drug resistance: relevance in targeted therapies for hepatocellular carcinoma, World J. Hepatol. 2 (2010) 114–126.
[6] A.A. Stavrovskaya, Cellular mechanisms of multidrug resistance of tumor cells, Biochemistry (Mosc) 65 (2000) 95–106.
[7] L. Yang, X. Liu, Z. Lu, J. Yuet-Wa Chan, L. Zhou, K.P. Fung, et al., Ursolic acid induces doxorubicin-resistant HepG2 cell death via the release of apoptosis-inducing factor, Cancer Lett. 298 (2010) 128–138.
[8] L. Fan, G. Sun, T. Ma, F. Zhong, W. Wei, Melatonin overcomes apoptosis resistance in human hepatocellular carcinoma by targeting survivin and XIAP, J. Pineal Res. 55 (2013) 174–183.
[9] R. O'Connor, The pharmacology of cancer resistance, Anticancer Res. 27 (2007) 1267–1272.
[10] S.Y. Lee, K.A. Yoon, S.H. Jang, E.O. Ganbold, D. Uuriintuya, S.M. Shin, et al., Infrared spectroscopy characterization of normal and lung cancer cells originated from epithelium, J. Vet. Sci. 10 (2009) 299–304.
[11] Z. Movasaghi, S. Rehman, D.I. ur Rehman, Fourier Transform Infrared (FTIR) spectroscopy of biological tissues, Appl. Spectrosc. Rev. 43 (2008) 134–179.
[12] G. Bellisola, C. Sorio, Infrared spectroscopy and microscopy in cancer research and diagnosis, Am. J. Cancer Res. 2 (2012) 1–21.
[13] S. Machana, N. Weerapreeyakul, S. Barusrux, K. Thumanu, W. Tanthanuch, FTIR microspectroscopy discriminates anticancer action on human leukemic cells by extracts of Pinus kesiya; Cratoxylum formosum ssp. pruniflorum and melphalan, Talanta 93 (2012) 371–382.
[14] M. Srisayam, N. Weerapreeyakul, S. Barusrux, W. Tanthanuch, K. Thumanu, Application of FTIR microspectroscopy for characterization of biomolecular changes in human melanoma cells treated by sesamol and kojic acid, J. Dermatol. Sci. 73 (2014) 241–250.
[15] K.R. Flower, I. Khalifa, P. Bassan, D. Démoulin, E. Jackson, N.P. Lockyer, et al., SynchrotronFTIR analysis of drug treated ovarian A2780 cells: an ability to differentiate cell response to different drugs? Analyst 136 (2011) 498–507.
[16] G. Bellisola, M. Della Peruta, M. Vezzalini, E. Moratti, L. Vaccari, G. Birarda, et al., Tracking InfraRed signatures of drugs in cancer cells by Fourier Transform microspectroscopy, Analyst 135 (2010) 3077.
[17] F. Draux, P. Jeannesson, C. Gobinet, J. Sule-Suso, J. Pijanka, C. Sandt, et al., IR spectroscopy reveals effect of non-cytotoxic doses of anti-tumour drug on cancer cells, Anal. Bioanal. Chem. 395 (2009) 2293–2301.
[18] Y.B. Xie, Q. Liu, F. He, C.G. Guo, C.F. Wang, P. Zhao, Diagnosis of colon cancer with Fourier transform infrared spectroscopy on the malignant colon tissue samples, Chin. Med. J. (Engl.) 124 (2011) 2517–2521.
[19] R. Mehrotra, G. Tyagi, D.K. Jangir, R. Dawar, N. Gupta, Analysis of ovarian tumor pathology by Fourier Transform Infrared Spectroscopy, J. Ovarian Res. 3 (2010) 27.
[20] M. Dimitrova, D. Ivanova, I. Karamancheva, A. Milev, I. Dobrev, Application of FTIR-spectroscopy for diagnosis of breast cancer tumors, J. Chem. Technol. 44 (2009) 297–300.
[21] J.S. Wang, J.S. Shi, Y.Z. Xu, X.Y. Duan, L. Zhang, J. Wang, et al., FT-IR spectroscopic analysis of normal and cancerous tissues of esophagus, World J. Gastroenterol. 9 (2003) 1897–1899.
[22] D. Ye, W. Tanthanuch, K. Thumanu, A. Sangmalee, R. Parnpai, P. Heraud, Discrimination of functional hepatocytes derived from mesenchymal stem cells using FTIR microspectroscopy, The Anal. 137 (2012) 4774.
[23] A. Zwielly, J. Gopas, G. Brkic, S. Mordechai, Discrimination between drug-resistant and non-resistant human melanoma cell lines by FTIR spectroscopy, Analyst 134 (2009) 294–300.
[24] A. Gaigneaux, J.M. Ruysschaert, E. Goormaghtigh, Infrared spectroscopy as a tool for discrimination between sensitive and multiresistant K562 cells, Eur. J. Biochem. 269 (2002) 1968–1973.
[25] C. Murali Krishna, G. Kegelaer, I. Adt, S. Rubin, V.B. Kartha, M. Manfait, et al., Characterisation of uterine sarcoma cell lines exhibiting MDR phenotype by vibrational spectroscopy, Biochim. Biophys. Acta 2005 (1726) 160–167.
[26] R. Zendehdel, A. Masoudi-Nejad, J. Mohammadzadeh, H.S.F. Cisplatin Resistant, Patterns in Ovarian Cell Line Using FTIR and Principle Component Analysis, Iran. J. Pharm. Res. 11 (2012) 235–240.
[27] Y. Zhou, X.L. Ling, S.W. Li, X.Q. Li, B. Yan, Establishment of a human hepatoma multidrug resistant cell line in vitro, World J. Gastroenterol. 16 (2010) 2291–2297.
[28] S. Machana, N. Weerapreeyakul, S. Barusrux, A. Nonpunya, B. Sripanidkulchai, T. Thitimetharoch, Cytotoxic and apoptotic effects of six herbal plants against the human hepatocarcinoma (HepG2) cell line, Chin. Med. 6 (2011) 39.
[29] T. Okura, M. Ibe, K. Umegaki, K. Shinozuka, S. Yamada, Effects of dietary ingredients on function and expression of P-glycoprotein in human intestinal epithelial cells, Biol. Pharm. Bull. 33 (2010) 255–259.
[30] J. Echevarria-Lima, F. Kyle-Cezar, P.L. DF, L. Capella, M.A. Capella, V. M. Rumjanek, Expression and activity of multidrug resistance protein 1 in a murine thymoma cell line, Immunology 114 (2005) 468–475.
[31] K. Mohankumar, S. Pajaniradje, S. Sridharan, V.K. Singh, L. Ronsard, A. C. Banerjea, et al., Mechanism of apoptotic induction in human breast cancer cell, MCF-7, by an analog of curcumin in comparison with curcumin—an in vitro and in silico approach, Chem. Biol. Interact. 210 (2014) 51–63.
[32] J.X. Yang, Y. Luo, H.M. Qiu, W.X. Tang, Characterization and resistance mechanisms of cisplatin-resistant human hepatocellular carcinoma cell line, Saudi Med. J. 30 (2009) 35–40.
[33] C. Verslype, O. Rosmorduc, P. Rougier, Hepatocellular carcinoma: ESMO-ESDO clinical practice guidelines for diagnosis, treatment and follow-up, Ann. Oncol. 23 (Suppl 7) (2012) vii41–vii48.
[34] A. Pasqualato, A. Palombo, A. Cucina, M.A. Mariggiò, L. Galli, D. Passaro, et al., Quantitative shape analysis of chemoresistant colon cancer cells: correlation between morphotype and phenotype, Exp. Cell Res. 318 (2012) 835–846.
[35] L. Galluzzi, L. Senovilla, I. Vitale, J. Michels, I. Martins, O. Kepp, et al., Molecular mechanisms of cisplatin resistance, Oncogene 31 (2011) 1869–1883.
[36] W. Gu, F.F. Fang, B. Li, B.B. Cheng, C.Q. Ling, Characterization and resistance mechanisms of a 5-fluorouracil- resistant hepatocellular carcinoma cell line, Asian Pac. J. Cancer Prev. 13 (2012) 4807–4814.
[37] M. Zandvliet, E. Teske, J.A. Schrickx, Multi-drug resistance in a canine lymphoid cell line due to increased P-glycoprotein expression, a potential model for drug-resistant canine lymphoma, Toxicol. Vitro 28 (2014) 1498–1506.
[38] R. Zhang, Y. Niu, Y. Zhou, Increase the cisplatin cytotoxicity and cisplatin-induced DNA damage in HepG2 cells by XRCC1 abrogation related mechanisms, Toxicol. Lett. 192 (2010) 108–114.
[39] A. Barth, Infrared spectroscopy of proteins, Biochim. Biophys. Acta (BBA) – Bioenergetics 1767 (2007) 1073–1101.
[40] L.M. Miller, P. Dumas, From structure to cellular mechanism with infrared microspectroscopy, Curr. Opin. Struct. Biol. 20 (2010) 649–656.
[41] A.M. Melin, A. Allery, A. Perromat, C. Bebear, G. Deleris, B. de Barbeyrac, Fourier transform infrared spectroscopy as a new tool for characterization of mollicutes, J. Microbiol. Methods 56 (2004) 73–82.
[42] C.M. Krishna, G. Kegelaer, I. Adt, S. Rubin, V.B. Kartha, M. Manfait, et al., Combined Fourier transform infrared and Raman spectroscopic approach for identification of multidrug resistance phenotype in cancer cell lines, Biopolymers 82 (2006) 462–470.
[43] M. Dong, L. Ladaviere, F. Penin, G. Deleage, L.G. Baggetto, Secondary structure of P-glycoprotein investigated by circular dichroism and amino acid sequence analysis, Biochim. Biophys. Acta 1371 (1998) 317–334.
[44] C. Vigano, M. Julien, I. Carrier, P. Gros, J.M. Ruysschaert, Structural and functional asymmetry of the nucleotide-binding domains of P-glycoprotein investigated by attenuated total reflection Fourier transform infrared spectroscopy, J. Biol. Chem. 277 (2002) 5008–5016.
[45] M.F. Rosenberg, A.B. Kamis, R. Callaghan, C.F. Higgins, R.C. Ford, Three-dimensional structures of the mammalian multidrug resistance P-glycoprotein demonstrate major conformational changes in the transmembrane domains upon nucleotide binding, J. Biol. Chem. 278 (2003) 8294–8299.
[46] L. Manciu, X.B. Chang, J.R. Riordan, J.M. Ruysschaert, Multidrug resistance protein MRP1 reconstituted into lipid vesicles: secondary structure and nucleotide-induced tertiary structure changes, Biochemistry 39 (2000) 13026–13033.